ELSEVIER

Nuclear Instruments and Methods in Physics Research A 476 (2002) 42–51

NUCLEAR INSTRUMENTS & METHODS IN PHYSICS RESEARCH Section A

www.elsevier.com/locate/nima

Measurement of the energy spectrum of cosmic-ray induced neutrons aboard an ER-2 high-altitude airplane

P. Goldhagen[a,*], M. Reginatto[a], T. Kniss[b], J.W. Wilson[c], R.C. Singleterry[c], I.W. Jones[c], W. Van Steveninck[a]

[a] *US Department of Energy, Environmental Measurements Laboratory, 201 Varick Street, 5th Floor, New York, NY 10014-4811, USA*
[b] *Keithley Instruments, Inc., 28775 Aurora Road, Cleveland, OH 44139, USA*
[c] *NASA Langley Research Center, Hampton, VA 23681-0001, USA*

Abstract

Crews working on present-day jet aircraft are a large occupationally exposed group with a relatively high average effective dose from galactic cosmic radiation. Crews of future high-speed commercial aircraft flying at higher altitudes would be even more exposed. To help reduce the significant uncertainties in calculations of such exposures, the atmospheric ionizing radiation (AIR) project, an international collaboration of 15 laboratories, made simultaneous radiation measurements with 14 instruments on five flights of a NASA ER-2 high-altitude aircraft. The primary AIR instrument was a highly sensitive extended-energy multisphere neutron spectrometer with lead and steel shells placed within the moderators of two of its 14 detectors to enhance response at high energies. Detector responses were calculated for neutrons and charged hadrons at energies up to 100 GeV using MCNPX. Neutron spectra were unfolded from the measured count rates using the new MAXED code. We have measured the cosmic-ray neutron spectrum (thermal to >10 GeV), total neutron fluence rate, and neutron effective dose and dose equivalent rates and their dependence on altitude and geomagnetic cutoff. The measured cosmic-ray neutron spectra have almost no thermal neutrons, a large "evaporation" peak near 1 MeV and a second broad peak near 100 MeV which contributes about 69% of the neutron effective dose. At high altitude, geomagnetic latitude has very little effect on the shape of the spectrum, but it is the dominant variable affecting neutron fluence rate, which was eight times higher at the northernmost measurement location than it was at the southernmost. The shape of the spectrum varied only slightly with altitude from 21 km down to 12 km (56–201 g cm^{-2} atmospheric depth), but was significantly different on the ground. In all cases, ambient dose equivalent was greater than effective dose for cosmic-ray neutrons. © 2002 Elsevier Science B.V. All rights reserved.

PACS: 87.53.Qc; 96.40.z

Keywords: Neutron spectrometry; Cosmic rays; Bonner spheres; Neutron dosimetry; Radiation protection

1. Introduction

The Earth is continually bathed in high-energy particles that come from outside the solar system, known as galactic cosmic rays. When these

*Corresponding author. Tel.: +1-212-620-3645; fax: +1-212-620-3600.
E-mail address: goldhagn@eml.doe.gov (P. Goldhagen).

0168-9002/02/$ -see front matter © 2002 Elsevier Science B.V. All rights reserved.
PII: S0168-9002(01)01386-9

particles penetrate the magnetic fields of the solar system and the Earth and reach the Earth's atmosphere, they collide with atomic nuclei in air and create cascades of secondary radiation of every kind [1]. The intensity of the different particles making up atmospheric cosmic radiation, their energy distribution, and their potential biological effect on aircraft occupants vary with altitude, location in the geomagnetic field, and time in the Sun's magnetic activity cycle [1–3]. The atmosphere provides shielding, which at a given altitude is determined by the mass thickness of the air above that altitude, called atmospheric depth. The geomagnetic field provides a different kind of shielding, by deflecting low-momentum charged particles back into space. The minimum momentum per unit charge (magnetic rigidity) a vertically incident particle can have and still reach a given location above the Earth is called the geomagnetic vertical cutoff rigidity (or simply cutoff) for that point. (Values of geomagnetic cutoff as a function of geographic location used in this paper are the ones used by recent versions of the CARI and LUIN codes [4,5].)

Over the past 10 years, there has been increasing concern about the exposure of air crews to atmospheric cosmic radiation [4,6,7]. At aviation altitudes, the neutron component of the secondary cosmic radiation contributes about half of the dose equivalent, but until recently it has been difficult to accurately calculate or measure the cosmic-ray neutron spectrum in the atmosphere to determine accurate dosimetry [7–11]. Dose rates from atmospheric cosmic radiation at commercial aviation altitudes are such that crews working on present-day jet aircraft are an occupationally exposed group with a relatively high average effective dose [2,4,7]. Crews of future high-speed commercial aircraft flying at higher altitudes would be even more exposed [8].

2. The atmospheric ionizing radiation (AIR) project measurements

To help reduce the significant uncertainties in calculations of such exposures, the AIR project, an international collaboration of 15 laboratories organized by the NASA Langley Research Center, made simultaneous radiation measurements with 14 instruments on a NASA ER-2 high-altitude aircraft [7]. Of the many AIR measurements, this paper discusses only the neutron spectrometry.

The AIR ER-2 flights were scheduled for June 1997, a time of maximum galactic cosmic radiation (solar minimum), and were designed to cover as wide a range of latitude and altitude as possible within the operational capabilities of the ER-2. There were five measurement flights. Their four paths (there were two identical South flights) are shown on a map in Fig. 1. All flights originated at the NASA Ames Research Center (37.4°N, 122°W) in California and started with a northward climb. The East flight provided a long period of nearly constant radiation level by flying at constant geomagnetic cutoff. The rest of the flights measured the effects of latitude and of altitude at low-geomagnetic cutoffs. The East and the two

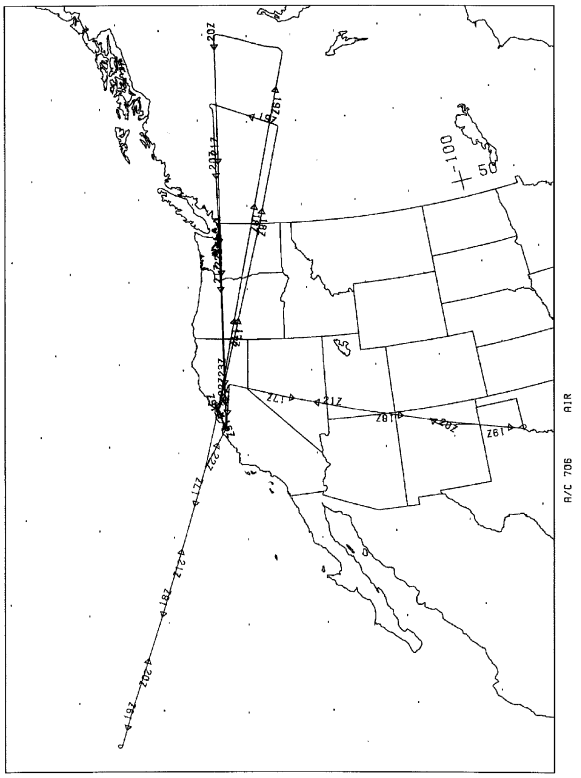

Fig. 1. Flight paths of the AIR measurement ER-2 flights.

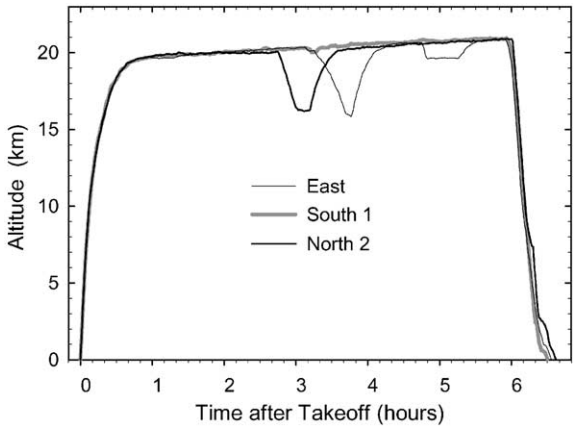

Fig. 2. Altitude as a function of time during three of the flights.

North flights included an altitude dip while flying magnetic west at constant geomagnetic cutoff, allowing measurements at altitudes from 21.3 km (70,000 ft) down to 16 km (52,500 ft). Fig. 2 shows graphs of altitude as a function of time after takeoff for three of the flights. Overall, the flights covered latitudes from 18° to 60°N, corresponding to geomagnetic vertical cutoff rigidities from 12 to 0.4 GV, and atmospheric depths from 50 to 110 g cm^{-2}, not including initial climb and final descent, which yield some data at lower altitudes for one latitude. Neutron spectrometry measurements were also made on the ground.

3. The high-energy multisphere neutron spectrometer

The primary AIR instrument was a highly sensitive extended-energy multisphere (Bonner sphere) neutron spectrometer (MNS) [12] designed specifically for cosmic-ray measurements [13,14]. Its 14 detectors are spherical 5.08 cm diameter ^{3}He-filled proportional counters, with one unshielded, one surrounded with a layer of cadmium, and the rest surrounded with high-density polyethylene spheres with diameters ranging from 6.7 to 38 cm. Moderator diameters and masses for all the detectors are given in Table 1. The large cross-sectional area of the ^{3}He proportional counters and simultaneous measurement with all the detectors gives the spectrometer high sensitivity. To reduce response to thermal neutrons, all but the largest moderator spheres are surrounded with thin cadmium shells. To meet the safety requirements for flight on the ER-2, each detector, together with its high-voltage supply and preamplifier, was enclosed in a cylindrical aluminum container sealed at atmospheric pressure. Detectors were placed in all four major payload bays of the ER-2. Due to space constraints, detectors 3 and 5 were not flown.

Table 1
Detector moderator diameters and masses

Detector no.	Outside diameter (in)	Outside diameter (cm)	Mass of polyethylene (kg)	Mass of converter shell (kg)
1 (bare)	—	—	—	—
2 (Cd)	—	—	—	—
3[a]	2.620	6.66	0.0773	—
4	3.234	8.21	0.2021	—
5[a]	3.849	9.78	0.3893	—
6	4.626	11.75	0.7306	—
7	5.626	14.29	1.3845	—
8	6.814	17.31	2.521	—
9	8.232	20.91	4.478	—
10	9.830	24.97	7.680	—
11	11.846	30.09	13.481	—
12	14.974	38.03	27.305	—
13	11.848	30.09	11.262	25.225 Pb
14	15.030	38.18	25.395	17.917 Fe

[a] Not flown because of ER-2 space constraints.

The signal processing and data acquisition electronics and methods were similar to those described for previous MNS measurements [13,15,16]. After passing through a preamplifier and a purpose-built amplifier [13], signals from each proportional counter were routed through one of a pair of 8-channel multiplexers to an analog to digital converter and the pulse height stored in a computer-card multichannel analyzer. Pulse-height spectra were recorded on the computer's magneto-optical disk every 60 s throughout each flight. Pulses as small as 5% of the peak pulse-height from ^{3}He(n, p)^{3}H thermal-neutron capture were recorded. During analysis, neutron capture pulses were cleanly separated from elec-

tronic noise and pulses from minimum ionizing particles by setting a software threshold at 24% of the peak pulse-height channel. The average in-flight cosmic-ray neutron count rate in the detectors was about 4 to 32 per s, allowing statistically sound spectra to be collected in a few minutes.

Even very large Bonner spheres with standard all-plastic moderators have responses that drop to low values as the energy increases from about 15 MeV to several hundred MeV (see Fig. 3, curves 8–12), so standard MNSs cannot be used to measure the shape of neutron spectra at energies much above 20 MeV. Following suggestions of Hsu et al. [17] based on work by Birattari et al. [18], the Environmental Measurements Laboratory developed high-energy detectors incorporating 1.65 cm thick metal shells within their polyethylene moderators. Detectors 13 and 14 have the same diameter moderators (30 and 38 cm) as detectors 11 and 12, but detector 13 has a 25 kg lead shell embedded in its moderator, and 14 has an 18 kg steel shell. High-energy neutrons striking the nuclei of atoms with high atomic number cause hadronic showers with easily detected secondary neutrons, creating a rising response with increasing energy (see Fig. 3, curves 13 and 14).

Detector responses as a function of energy (see Figs. 3 and 4) were calculated for neutrons at energies up to 150 MeV using MCNP (version 4b) [19] and MCNPX (version 2.1.5, 19th March 2000) [20,21] with evaluated cross sections [19,22] and for neutrons, protons and charged pions from 10 MeV to 100 GeV using MCNPX with cross sections from nuclear models (see Fig. 5). The methods used with MCNP have been described previously [16,23] and are similar to those used by Mares et al. [24,25]. We used a continuous distribution of incident energy, with the results grouped into 20 equal-log(E)-width bins per energy decade. The dips in response at neutron energies near 10^{-4} and 10^{-1} MeV come from nuclear resonances in the cadmium shells and aluminum surrounding the spheres. Of the high-energy nuclear models currently available in MCNPX, we chose the Bertini model with preequilibrium from 150 MeV to 3.5 GeV and the

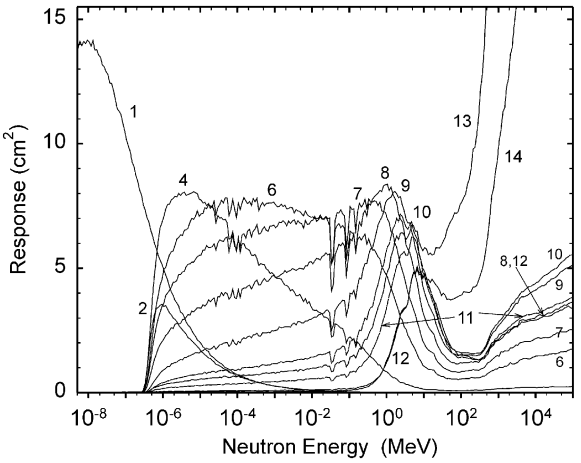

Fig. 3. Calculated neutron response functions for each of the detectors of the EML high-energy multisphere spectrometer.

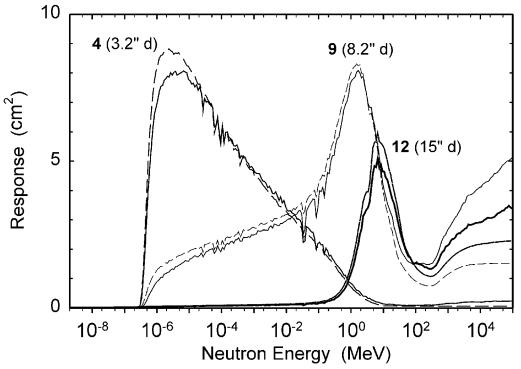

Fig. 4. Calculated neutron response functions for a small, medium and large detector of the MNS with (solid curves) and without (dashed curves) including the containers, other detectors and surrounding materials in the response calculation.

"scaled Bertini" model above 3.5 GeV. We did not use the "Fluka model" in MCNPX because it is from an early version of the FLUKA code [26] which gives very different answers [27] from more recent versions. From 10 to 150 MeV, we had a choice of results for our neutron response functions. For detectors 1–13, we chose the results from MCNPX with evaluated cross sections. For detector 14, with its steel shell, we used the results

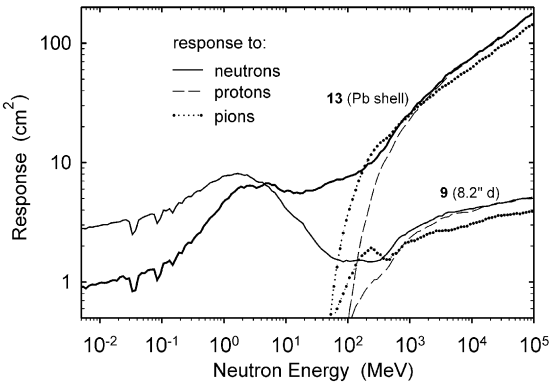

Fig. 5. Calculated neutron, proton and charged pion response functions for detectors 9 (8.2″ diameter moderator) and 13 (11.8″ moderator with 25 kg embedded lead shell). Surrounding materials were included in the calculations.

from the Bertini model starting at 70 MeV because above that energy the evaluated cross sections for iron give evaporation neutron yields higher than experimental data ([22], Fig. 24a). (Shortly before this Workshop, we learned of an experiment [28] showing that the Bertini model with preequilibrium overestimates the yield of moderatable neutrons from protons on lead by about 13% at incident energies from 0.5 to 1.4 GeV. This means our response function for detector 13 may be too high by a similar amount in this energy region.) The effects of the various materials surrounding each detector were included in the response calculations by modeling the entire assembly of AIR apparatus in each ER-2 payload bay. Fig. 4 shows the neutron response functions of three of the detectors with and without including the effects of nearby materials. Response decreased at low energies because of shielding effects and increased at high energies because of hadron showers in surrounding metals. We have verified our response calculations at fission energies to within 4% using measurements of a calibrated ^{252}Cf neutron source [23]. An experiment to verify the calculated responses in the energy range 150–700 MeV has been performed at the Los Alamos Neutron Science Center, but has not yet been analyzed.

For all the larger detectors, the raw count rates must be corrected for counts caused by high-energy cosmic-ray protons and pions, which produce neutrons by nuclear interactions with the metals and carbon in the detectors and their surroundings. This requires calculating response functions for these particles as well as for neutrons and knowing their (approximate) cosmic-ray spectra. Fig. 5 compares calculated neutron, proton and charged pion response functions for detectors 9 and 13. Surrounding materials were included in the calculations. At present, the only available calculation of proton and pion cosmic-ray spectra for all locations in the atmosphere is from the LUIN code [5,29]. This analytic radiation transport code relies on several approximations which are valid only above several hundred MeV, but it is still widely used (within the CARI code [4]) for aircraft route dose calculations. There is also a recent Monte Carlo calculation of cosmic radiation in the atmosphere [10] that includes proton and pion spectra at one location (at 200 g cm^{-2} above Braunschweig, Germany). We calculated the count rates that would occur in our detectors at this location assuming the charged hadron fluence spectra calculated by Kurochkin et al. [10] and by using LUIN-99 [5], and found the former to be 1.22 times the latter. To estimate the charged-hadron count rates present in the AIR MNS measurements, we used 1.11 times the proton plus pion counts predicted by the LUIN spectra at each measurement location folded with our calculated proton and pion response functions. This charged-hadron count rate was subtracted from the raw count rate to get the neutron count rate.

Once the neutron count rates and response functions of the MNS detectors are known, a deconvolution (unfolding) computer code is applied to determine the neutron spectrum. The deconvolution process is not straightforward because information in addition to the measurement and the response functions must be applied to obtain a unique solution. We use the unfolding code MAXED [30–32], which takes into account the individual uncertainties in the detector count rates and allows for the inclusion of a priori information in a well defined and mathematically consistent way. The a priori information is in the form of an initial (default) spectrum that

represents knowledge about the spectrum before the measurement is made [30]. Since MAXED applies no smoothing, it preserves any structure in the default spectrum that is finer than the resolution of the spectrometer.

4. Measured cosmic-ray neutron spectra

As initial spectra for unfolding our measurements and for comparison with them, we examined available calculated cosmic-ray neutron spectra. Fig. 6a shows graphs of three calculated cosmic-ray neutron spectra for different locations in the atmosphere made by different groups [9,10,33] using different Monte Carlo radiation transport codes. Neutron fluence rate (neutrons $cm^{-2}s^{-1}$) per lethargy (the natural logarithm of energy) is plotted on the vertical axis versus neutron energy in MeV with a logarithmic scale on the horizontal axis. (Fluence rate per lethargy is equivalent to $E(d\phi/dE)$, where E is particle energy and ϕ the fluence rate.) The calculated spectra have been scaled to fit one of our measurements (see below), so they overlap and their shape can be compared. The calculated spectra all have a large "evaporation" peak centered at 1 or 2 MeV, a smaller peak at about 100 MeV, and detectable numbers of neutrons up to about 10 GeV (10^4 MeV). The spectrum of Roesler et al. [9], calculated for 200 g cm^{-2} at 4.3 GV cutoff, shows fine structure from nuclear resonances in the nitrogen and oxygen of the atmosphere. It also has a larger ratio of high-energy neutrons to evaporation neutrons than the calculations by Kurochkin et al. [10] (200 g cm^{-2}, 2.9 GV cutoff) and by Armstrong et al. [33] (50 g cm^{-2}, 4.6 GV cutoff). Only the Armstrong calculation included thermal energies.

Fig. 6b shows cosmic-ray neutron spectra unfolded from our MNS measurements at one location using each of the calculated spectra in Fig. 6a as the default spectrum. (The Armstrong thermal tail was attached to the other two calculated spectra before unfolding.) Except for their bin structure, the three unfolded spectra are practically identical, and we can refer to any of them as the measured spectrum. The measured

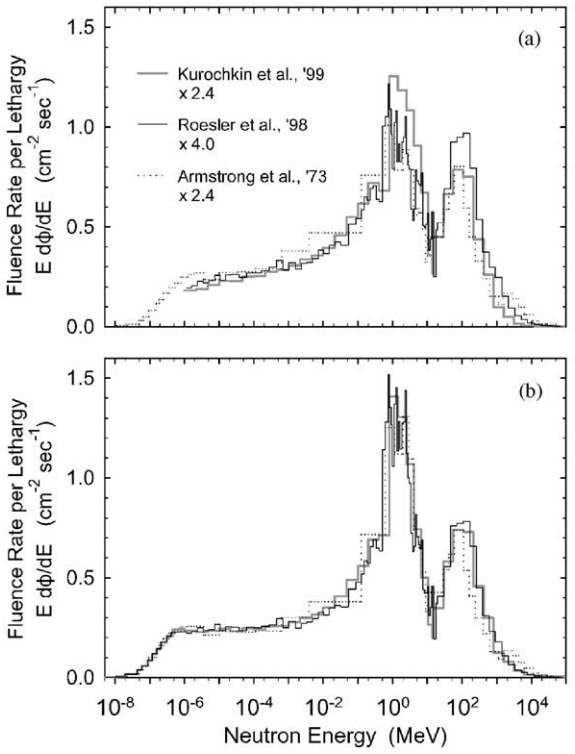

Fig. 6. (a) Three calculated cosmic-ray neutron spectra [9,10,33] used as default spectra in unfolding the measured spectra. The calculated spectra are shown scaled to give the best fit to the data used to unfold the spectra in (b). (b) Cosmic-ray neutron spectra unfolded from measurements at high altitude and high northern latitude (56 g cm^{-2} atmospheric depth, 20 km altitude; 54°N, 117°W, 0.8 GV geomagnetic cutoff) using each of the calculated spectra in (a) as the default spectrum.

spectrum is generally similar to the calculated spectra, but it has a taller evaporation neutron peak and is lower from 10^{-4} to 0.2 MeV. The measured spectrum has a smaller 100 MeV peak than the Roesler spectrum, a wider valley between the two peaks than the Kurochkin spectrum, and almost no thermal neutrons.

When the calculated spectra are scaled (without changing their shapes, as in Fig. 6a) to fit the measured neutron count rates, the Roesler and Kurochkin spectra fit better than the Armstrong spectrum (reduced $\chi^2 = 9.8$, 10.6, and 18.2, respectively). In the rest of the figures in this paper, we show measured spectra unfolded using the Kurochkin rather than the Roesler spectrum as the

default spectrum only because the former's simpler structure facilitates visual comparisons.

The data unfolded in Fig. 6b were taken on the shorter North flight near the northern extreme of its outbound leg (54°N, 117°W, cutoff = 0.8 GV) at an atmospheric depth of $56\,g\,cm^{-2}$ (20 km (65,600 ft) altitude). Over 2×10^5 neutron counts were recorded in 10 min. Fig. 7 shows the same measured spectrum together with a spectrum measured for 24 min near the southern extreme of the South 1 flight (18.7°N, 127°W, 12 GV cutoff) at almost the same atmospheric depth ($53.5\,g\,cm^{-2}$, 20.3 km). The total neutron fluence rate at the northern location was eight times the fluence rate at the southern location; the southern spectrum is shown multiplied by 8. The spectra have almost the same shape. What difference there is may be due to the lower statistics of the southern measurement and the relatively large uncertainty of the correction for charged hadrons when applied to two locations with such different geomagnetic cutoffs.

Fig. 8 shows cosmic-ray neutron spectra measured at three different altitudes on the ER-2 and on the ground. The locations, atmospheric depths, and altitudes of the measurements are given in Table 2. The measurement at $56\,g\,cm^{-2}$ (dotted line) is the same northern spectrum shown in Figs. 7 and 6b. At $101\,g\,cm^{-2}$, the atmospheric depth is 1.8 times greater, but the total neutron fluence rate decreased by less than 3%. The small difference between the spectral shapes at 56 and $101\,g\,cm^{-2}$ is large enough to affect the ratio of dosimetric quantities to total neutron fluence. The difference is probably real, because the two measurements were taken on the same flight with nearly the same total counts and count rate at nearly the same cutoff. The difference between the spectrum measured at $201\,g\,cm^{-2}$ (11.9 km, 39,000 ft) and the spectra at higher altitudes may be within our uncertainties. The measurement at $201\,g\,cm^{-2}$ was taken by combining 2 min of data from each of four flights as the ER-2 rapidly climbed through normal commercial aviation altitudes shortly after takeoff (see Fig. 2). About 54,000 neutron counts were recorded in those 8 min. The cosmic-ray neutron spectrum measured on the ground shows a distinctly different shape,

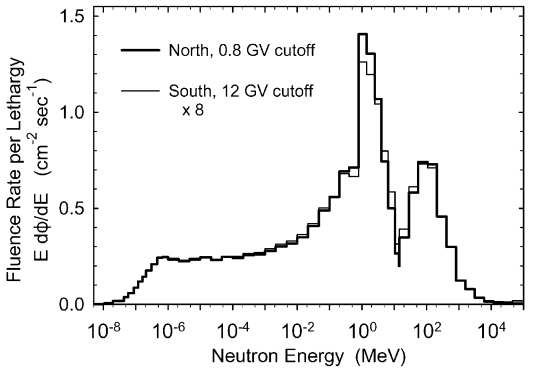

Fig. 7. Cosmic-ray neutron spectra measured at the same northern location as in Fig. 6b and at the south end of the South-1 flight (19°N, 127°W, 12 GV cutoff; $54\,g\,cm^{-2}$ atmospheric depth). The south spectrum is shown multiplied by 8.

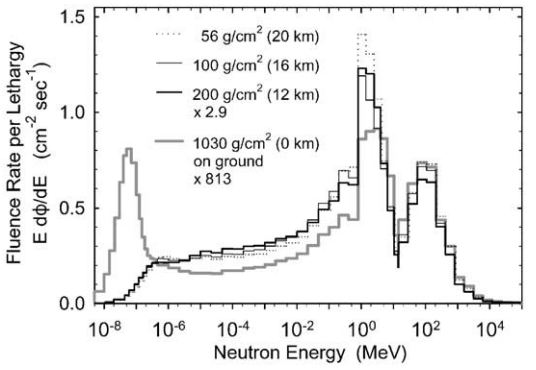

Fig. 8. Comparison of cosmic-ray neutron spectra measured at different atmospheric depths (altitudes) during the ER-2 flights and on the ground at sea level.

because soil reflects neutrons differently than air does. As expected, a significant number of thermal neutrons is produced in the ground. Normalized to the same total fluence rate as the in-flight measurements, the ground spectrum is lower from 10^{-6} to 2 MeV and enhanced or the same at higher energies. The data for the ground measurement shown were collected for a week and had about 2.1×10^5 neutron counts.

5. Dosimetric results and discussion

Total fluence, effective dose, and ambient dose equivalent ($H^*(10)$) rates have been determined

Table 2
Neutron integral quantities measured at various locations

Geographic location	Cutoff (GV)	Atmospheric depth ($g\,cm^{-2}$)	Altitude		Neutron fluence rate ($cm^{-2}\,s^{-1}$)	Effective dose rate ($\mu Sv\,h^{-1}$)	$H^*(10)$ Rate ($\mu Sv\,h^{-1}$)
			(km)	(ft)			
19°N, 127°W	12	53.5	20.3	66,500	1.28	0.91	1.06
54°N, 117°W	0.8	56	20.0	65,600	10.2	6.9	8.5
56°N, 121°W	0.7	101	16.2	53,300	10.0	6.2	7.8
38°N, 122°W	4.5	201	11.9	39,000	3.4	2.1	2.7
37°N, 76°W	2.7	1030	0	0	0.0122	0.0083	0.0093

from the cosmic-ray neutron spectra measured at the five locations analyzed so far. The results for these integral quantities are given in Table 2. These values are the mean of the two values obtained from measured spectra unfolded using the Roesler and Kurochkin calculated spectra as default spectra, although no integral quantity differed by more than 3.3% between the two unfolded spectra. We used the neutron fluence to effective dose (isotropic irradiation) and $H^*(10)$ conversion factors from ICRU Report 57 [34] up to 20 and 201 MeV, respectively, and from Ferrari and colleagues [35,36] above those energies. Ambient dose equivalent was always greater than effective dose. For the high-altitude spectra, neutrons with energies >10 MeV made up 24% of the total fluence rate and contributed 38–39% of $H^*(10)$ and 68–70% of the effective dose rates. The high-energy fractions were slightly lower at 201 $g\,cm^{-2}$ (22%, 36%, 66%) and higher on the ground (25%, 44%, 72%).

Our work presents the first MNS measurements of cosmic-ray neutrons to make a correction for response to associated charged hadrons. Fig. 9 shows the measured neutron spectrum at 56 $g\,cm^{-2}$ with and without the correction for protons and pions. The proton spectrum used for the correction is also shown. The total fluence rate of the uncorrected neutron spectrum is too high by 7%. Since all of the excess is at high energy, the uncorrected $H^*(10)$ and effective dose rates are too high by 11% and 51%. Clearly, the effect of charged hadrons should not be ignored in measurements of this kind. Since our correction for charged hadrons is based on LUIN and a calculation at one location that differs from it by 22%, the estimated uncertainty in our correction is roughly $\pm 20\%$, and the propagated uncertainties in $H^*(10)$ and effective dose are $\pm 2\%$ and $\pm 10\%$. New calculations by Roesler et al. [11] should soon provide us with better atmospheric cosmic-ray particle spectra at several locations, which we can use for default neutron spectra in our unfolding as well as improved charged-hadron correction.

When comparing our measured cosmic-ray neutron spectra to similar measurements by others, e.g. [37], note that if the unfolding is cut off much below 10 GeV, especially if the effect of charged hadrons is ignored, the high-energy neutron peak can be surprisingly enlarged. Fig. 9 shows a spectrum unfolded from our uncorrected data while limiting the energy to <1 GeV.

6. Summary and conclusions

We summarize our results at the five locations analyzed so far as follows. At high altitude, geomagnetic latitude has very little effect on the shape of the spectrum, but it is the dominant variable affecting neutron fluence rate, which was eight times higher at the northernmost measurement location than it was at the southernmost. The shape of the cosmic-ray neutron spectrum varies only slightly with altitude from 21 km down to 12 km (56–201 $g\,cm^{-2}$ atmospheric depth), but is significantly different on the ground. In all cases, ambient dose equivalent was greater than effective dose for cosmic-ray neutrons. These are very encouraging results for those who are modeling

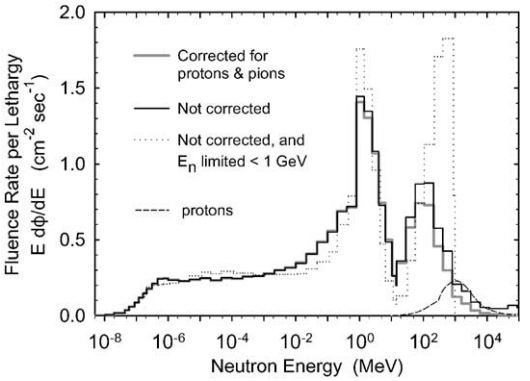

Fig. 9. Measured cosmic-ray neutron spectra before and after making the correction for counts caused by protons and pions. The proton spectrum used to make the correction is also shown, as is the effect of limiting the maximum neutron energy to 1 GeV.

and measuring air crew doses. They strongly suggest that the shape of the neutron spectrum is constant everywhere commercial aircraft now fly and allow the use of relatively simple measurements of $H^*(10)$ as a conservative estimator of neutron effective dose.

Only a small sample of the AIR MNS data have yet been analyzed. With further analysis, we will have a database of cosmic-ray neutron spectra and associated dosimetric quantities at solar minimum for a wide range of latitudes at high altitude, one latitude at commercial aviation altitudes, and for several times in the solar cycle at several latitudes and altitudes on the ground. The results can be used to verify, and if necessary, correct cosmic-ray transport calculations used to determine air crew doses. In addition, the results have applications in radiation effects on microelectronics, in determining source terms for cosmogenic nuclides used for atmospheric tracers and geological dating, and in evaluation of the background radiation exposure of the world population.

Acknowledgements

This work was supported by the High Speed Research Projects Office (HSRPO) of the NASA Langley Research Center, with additional support from the US Department of Energy. We thank D. Maiden and the rest of the HSRPO, the NASA technicians and engineers, and the ER-2 pilots, ground crew, and liaison staff for making the flights possible and successful. We thank H. Tai, J.L. Shin, F. Hajnal, M. Sims and L. Waters and the MCNPX development team. We thank T. Armstrong, K. Copeland, W. Friedberg, V. Mares, K. O'Brien, R. Prael, S. Roesler, B. Wiegel and H. Beck for results of their calculations and valuable discussions.

References

[1] G. Reitz, Radiat. Prot. Dosim. 48 (1993) 5.
[2] J.W. Wilson, Health Phys. 78 (2000) 470.
[3] W. Heinrich, S. Roesler, H. Schraube, Radiat. Prot. Dosim. 86 (1999) 253.
[4] K. O'Brien, F. Friedberg, F.E. Duke, L. Snyder, E.B. Darden, H.H. Sauer, Radiat. Prot. Dosim. 45 (1992) 145. CARI is available at http://www.cami.jccbi.gov/aam-600/ under Radiobiology Research team.
[5] K. O'Brien, LUIN-99 code, private communication.
[6] G. Reitz, K. Schnuer, K. Shaw (Eds.), Proceedings of the Workshop on Radiation Exposure of Civil Aircrew, Luxembourg, 25–27 June 1991, Radiat. Prot. Dosim. 48 (1993).
[7] P. Goldhagen, Health Phys. 78 (2000) 526.
[8] J.W. Wilson, J.E. Nealy, F.A. Cucinotta, J.L. Shinn, F. Hajnal, M. Reginatto, P. Goldhagen, NASA Technical Paper 3524 (1995), National Technical Information Service, Springfield, Virginia.
[9] S. Roesler, W. Heinrich, H. Schraube, Radiat. Res. 149 (1998) 87.
[10] A. Kurochkin, B. Wiegel, B.R.L. Siebert, Radiat. Prot. Dosim. 83 (1999) 281.
[11] S. Roesler, W. Heinrich, H. Schraube, Radiat. Res. (2001), submitted.
[12] D.J. Thomas, A.V. Alevra, Nucl. Instr. and Meth. A 476 (2002) 31, these proceedings.
[13] P. Goldhagen, W. Van Steveninck, in: Environmental Measurements Laboratory Annual Report—Calendar Year 1994, USDOE Report EML-571, New York, NY, USA, 1995, p. 30.
[14] P. Tume and 14 others, Proceedings of the American Nuclear Society 1996 Topical Meeting, Radiation Protection and Shielding, North Falmouth, MA, USA, 21–25 April 1996, American Nuclear Society, La Grange Park, IL, USA, 1996, p. 68.
[15] W.F. Harvey, F. Hajnal, Radiat. Prot. Dosim. 50 (1993) 13.
[16] P. Goldhagen, M. Reginatto, F. Hajnal, in: Proceedings of the American Nuclear Society 1996 Topical Meeting,

Radiation Protection and Shielding, North Falmouth, MA, USA, 21–25 April 1996, American Nuclear Society, La Grange Park, IL, USA, 1996, p. 139.
[17] H.H. Hsu, K.R. Alvar, D.G. Vasilik, IEEE Trans. Nucl. Sci. 41, 4 Part 1 (1994) p. 938.
[18] C. Birattari, A. Ferrari, C. Nuccetelli, M. Pelliccioni, M. Silari, Nucl. Instr. and Meth. A 297 (1990) 250.
[19] J.F. Briesmeister (Ed.), Los Alamos National Laboratory Report LA-12625-M, Los Alamos, NM, USA, 1997.
[20] H.G. Hughes, R.E. Prael, R.C. Little, Los Alamos National Laboratory Report XTM-RN (U)97-012, Los Alamos, NM, USA, 1997.
[21] L.S. Waters (Ed.), Los Alamos National Laboratory Report LA-UR 99-6058, Los Alamos, NM, USA, http://mcnpx.lanl.gov/, "MCNPX User's Manual", 1999.
[22] M.B. Chadwick, P.G. Young, S. Chiba, S.C. Frankle, G.M. Hale, H.G. Hughes, A.J. Koning, R.C. Little, R.E. MacFarlane, R.E. Prael, L.S. Waters, Nucl. Sci. Eng. 131 (1999) 293.
[23] T.A. Kniss, Thesis, University of Akron, Akron, OH, USA, 1996.
[24] V. Mares, G. Schraube, H. Schraube, Nucl. Instr. and Meth. A 307 (1991) 398.
[25] V. Mares, A. Sannikov, H. Schraube, in: Proceedings of the Third Specialist Meeting on Shielding Aspects of Accelerators, Targets and Irradiation Facilities, 12–13 May 1997, Sendai, Japan, OECD Nuclear Energy Agency, 1997.
[26] P.A. Aarnio et al., "FLUKA89," CERN informal report, January 2, 1990.
[27] R.E. Prael, private communication.
[28] M.S. Zucker, N. Tsoupas, P.E. Vanier, U. von Wimmersperg, S.F. Mughabghab, E. Schmidt, Nucl. Sci. Eng. 129 (1998) 180.
[29] K. O'Brien, USDOE EML-338, update of HASL-275, New York, NY, USA, 1978, available from: National Technical Information Service, Springfield, VA, USA.
[30] M. Reginatto, P. Goldhagen, USDOE Report EML-595, New York, NY, USA, 1998. Available at http://www.eml.doe.gov/publications/reports/
[31] M. Reginatto, P. Goldhagen, Health Phys. 77 (1999) 579.
[32] M. Reginatto, P. Goldhagen, S. Neumann, Nucl. Instr. and Meth. A 476 (2002) 242, these proceedings.
[33] T.W. Armstrong, K.C. Chandler, J. Barish, J. Geophys. Res. 78 (1973) 2715.
[34] International Commission on Radiation Units and Measurements, ICRU Report 57, ICRU, Bethesda, MD, USA, 1998.
[35] A. Ferrari, M. Pellicioni, M. Pillon, Radiat. Prot. Dosim. 71 (1997) 165.
[36] A. Ferrari, M. Pellicioni, Radiat. Prot. Dosim. 76 (1998) 215.
[37] H. Schraube, A. Jakes, A. Sannikov, E. Weitzenegger, S. Roesler, W. Heinrich, Radiat. Prot. Dosim. 70 (1997) 405.